

ARTICLE OPEN



Tuning magnetic confinement of spin-triplet superconductivity

Wen-Chen Lin^{1,7}, Daniel J. Campbell^{1,7}, Sheng Ran^{1,2,3}, I-Lin Liu^{1,2,3}, Hyunsoo Kim¹, Andriy H. Nevidomskyy⁴, David Graf⁵, Nicholas P. Butch^{1,2} and Johnpierre Paglione^{1,3,6}✉

Electrical magnetoresistance and tunnel diode oscillator measurements were performed under external magnetic fields up to 41 T applied along the crystallographic b axis (hard axis) of UTe_2 as a function of temperature and applied pressures up to 18.8 kbar. In this work, we track the field-induced first-order transition between superconducting and magnetic field-polarized phases as a function of applied pressure, showing suppression of the transition with increasing pressure until the demise of superconductivity near 16 kbar and the appearance of a pressure-induced ferromagnetic-like ground state that is distinct from the field-polarized phase and stable at zero field. Together with evidence for the evolution of a second superconducting phase and its upper critical field with pressure, we examine the confinement of superconductivity by two orthogonal magnetic phases and the implications for understanding the boundaries of triplet superconductivity.

npj Quantum Materials (2020)5:68; <https://doi.org/10.1038/s41535-020-00270-w>

INTRODUCTION

Previous work on uranium-based compounds, such as UGe_2 , URhGe , and UCoGe , has unearthed a rich interplay between superconductivity and ferromagnetism in this family of materials¹, with suggestions that ferromagnetic spin fluctuations can act to enhance pairing². The recent discovery of superconductivity in UTe_2 has drawn strong attention owing to a fascinating list of properties—including the absence of magnetic order at ambient pressure³, Kondo correlations, and extremely high upper critical fields⁴—that have led to proposals of spin-triplet pairing^{4–7}, and a chiral order parameter^{8,9}.

In addition, at least two forms of re-entrant superconductivity have been observed in high magnetic fields, including one that extends the low-field superconducting phase upon precise field alignment along the crystallographic b axis¹⁰, and an extreme high-field phase that onsets in pulsed magnetic fields above the paramagnetic normal state at angles tilted away from the b axis¹¹.

Applied pressure has also been shown to greatly increase the superconducting critical temperature T_c in UTe_2 ^{12,13}, from 1.6 K to nearly double that value near 10 kbar, and to induce a second superconducting phase above a few kbar¹³. Upon further pressure increase, evidence of suppression of the Kondo energy scale leads to an abrupt disappearance of superconductivity and a transition to a ferromagnetic phase¹². Together with the ambient pressure magnetic field-induced phenomena^{10,11,14,15}, the axes of the magnetic field, temperature, and pressure provide for a very rich and interesting phase space in this system. One of the key questions is in regard to the field-polarized (FP) phase that appears to truncate superconductivity at 34.5 T under proper b -axis field alignment^{10,11}, in particular regarding the nature of the coupling of the two phases and whether superconductivity could persist to even higher fields in the absence of the competing FP phase. The relation between the FP phase and the pressure-induced magnetic phase, which also competes with superconductivity¹¹, is similarly not yet fully understood.

In this work, we perform magnetoresistance (MR) and tunnel diode oscillator (TDO) measurements under both high hydrostatic pressures P and high magnetic fields H along the crystallographic b axis to explore the (H, T, P) phase diagram. We find that the FP phase that interrupts superconductivity at ambient pressure is strengthened with increasing pressure, so as to suppress the transition field until there is no trace of superconductivity down to 0.4 K above 16 kbar. At higher pressures, we find evidence of a distinct magnetic phase that appears to be ferromagnetic in nature and is also bordered by the FP phase at finite fields. Together with previous observations at ambient pressure, these results suggest a spectrum of magnetic interactions in UTe_2 and a multifaceted ground state sensitive to several physical tuning parameters.

RESULTS AND DISCUSSION

Experimental results

The magnetic field response of electrical resistance R at low pressures is similar to previous results at ambient pressure, which showed that the superconducting state persists up to the FP phase transition H^* of nearly 35 T for $H||b$, and re-entrant behavior can be observed near T_c for a slight misalignment of the field¹⁰. While it is not presently known why the b -axis alignment is crucial, it is thought that alignment of the applied field and fluctuating moments plays an important role^{10,11}. As shown in Fig. 1a, application of 4 kbar of pressure reduces the cut-off field H^* to 30 T at 0.38 K ($T_c = 1.7$ K without applied field) but retains the very sharp transition to the FP state, above which a negative MR ensues. Upon temperature increase, a re-entrant feature emerges below H^* similar to the previous reports¹⁰ but only above about 1.3 K, indicating either nearly perfect alignment along the b axis or reduced sensitivity to field angle at finite pressures.

Upon further pressure increase, T_c increases as previously shown^{12,13}, up to 2.6 K and 2.8 K at 8.5 kbar and 14 kbar, respectively. However, H^* is continuously reduced through this

¹Maryland Quantum Materials Center, Department of Physics, University of Maryland, College Park, MD 20742, USA. ²NIST Center for Neutron Research, National Institute of Standards and Technology, Gaithersburg, MD 20899, USA. ³Department of Materials Science and Engineering, University of Maryland, College Park, MD 20742, USA. ⁴Department of Physics and Astronomy, Rice University, Houston, TX 77005, USA. ⁵National High Magnetic Field Laboratory, Florida State University, Tallahassee, FL 32313, USA. ⁶Canadian Institute for Advanced Research, Toronto, Ontario M5G 1Z8, Canada. ⁷These authors contributed equally: Wen-Chen Lin, Daniel J. Campbell. ✉email: paglione@umd.edu

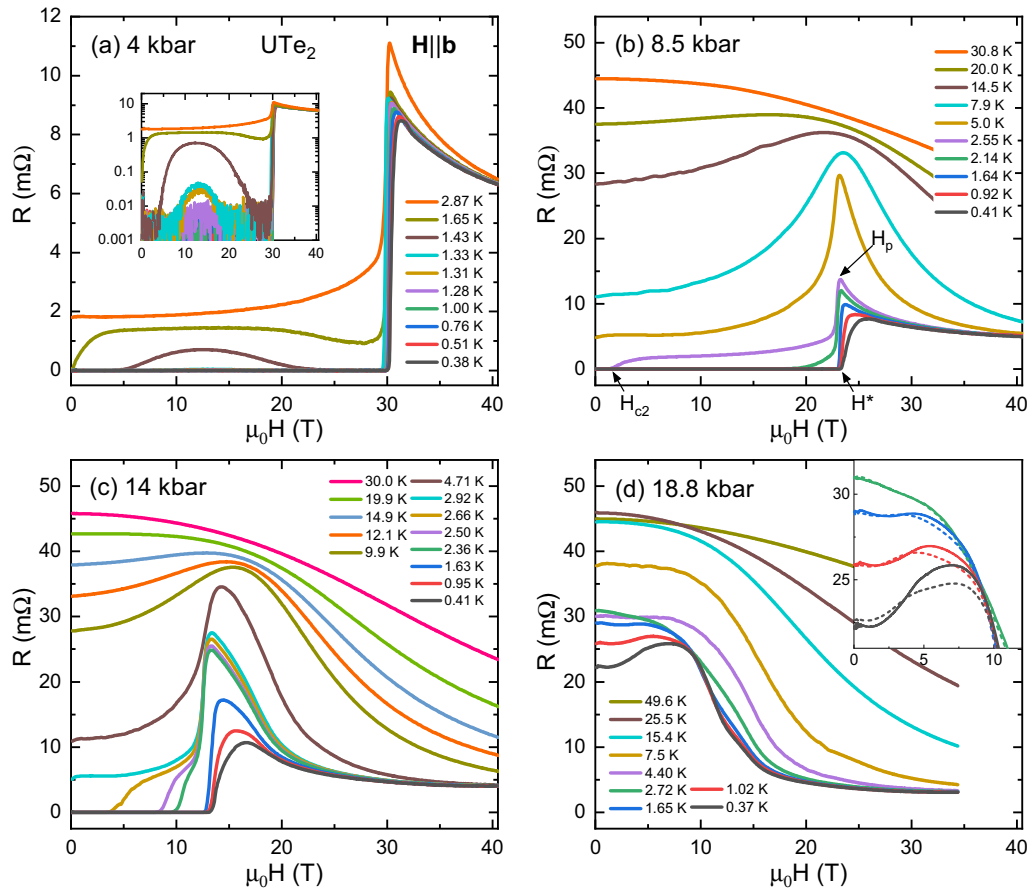


Fig. 1 Magnetoresistance of UTe_2 under applied pressures. Magnetoresistance of a UTe_2 single crystal with current applied along crystallographic a axis and magnetic fields applied along the b axis under applied pressures of (a) 4 kbar, (b) 8.5 kbar, (c) 14 kbar, and (d) 18.8 kbar. Inset of (a) shows a semilog plot of magnetoresistance at 4 kbar, highlighting re-entrant superconductivity. In panel (b), the applied field at the resistance peak (H_p) and the critical field (H_{c2}) are labeled on the violet curve as an example. The cut-off field (H^*) at base temperature is also labeled. Inset of (d) presents a zoom in the range where hysteresis is observed via distinct upsweep (solid lines) and downsweep (dashed lines) curves.

range and changes in character. As shown in Fig. 1b and c, at higher pressures H^* and H_{c2} dissociate, beginning as a single sudden rise with a broadened peak (denoted H_p) in resistance at 0.4 K that becomes better-defined upon increasing from lowest temperature, before separating into two distinct transitions at higher temperatures. Interestingly, the transition is the sharpest when the H_{c2} transition separates from H^* and moves down in the field. Further, the coupled transitions slightly decrease in the field until about 2 K, above which the resistive H_{c2} continues to decrease while H^* stalls (e.g., at about 12 T for 14 kbar) until washing out above ~ 20 K. This indicates a strong coupling between the two transitions that is weakened both on pressure increase and temperature increase, despite the first-order nature of the FP phase. At 18.8 kbar, shown in Fig. 1d, where no superconducting phase is observed down to 0.37 K, the sharp feature associated with H^* is gone, and only a broad maximum in R remains near 8 T. Around this feature, we observed hysteresis loops at low temperature as shown in the inset (see Supplementary Fig. 6 for hysteresis loops under both positive and negative fields). Together with the evidence from previous pressure experiments identifying similar hysteretic behavior¹², we believe there is a ferromagnetic-like ground state that evolves from zero temperature and zero magnetic field, and, similar to superconductivity at lower pressures, is truncated by the FP phase and therefore distinct from that ground state. The crossover from the FM-like ground state to the FP phase is also supported by the drop of resistance at around 10 T.

Figure 2 presents the frequency variation Δf in the TDO signal, where a minus sign has been applied to the frequency following convention. The frequency variations reflect the changes in magnetic susceptibility and therefore are sensitive to the anomalies that cannot be captured through transport measurements in the zero-resistance regime. In addition to a sharp rise in Δf at H^* , which corresponds to a diamagnetic to paramagnetic transition, and changes in slope consistent with the re-entrant behavior mentioned above (see Supplementary Fig. 4), there is another feature in the 4 kbar data within the superconducting state observable at lower fields. At temperatures below 1 K, Δf initially increases with field before abruptly transitioning to a constant above a characteristic field $H_{c2(2)}$, and finally jumping at the H^* transition. As the temperature is increased, $H_{c2(2)}$ decreases in field value until it vanishes above T_c , tracing out an apparent phase boundary within the superconducting state. As shown in Fig. 3, the path of $H_{c2(2)}$ merges with the zero-field critical temperature of the second superconducting phase “SC2” discovered by ac calorimetry measurements¹³. As shown in Fig. 3a, these data identify SC2 as having a distinct $H_{c2}(T)$ -phase boundary from the higher- T_c “SC1” phase, with a zero-temperature upper critical field of ~ 11 T at 4 kbar. Upon further pressure increase, the $H_{c2(2)}$ transition is suppressed in field, tracing out a reduced SC2 phase boundary (see Supplementary Fig. 3) that is absent by 14 kbar. In essence, it appears that the SC2 phase is suppressed more rapidly than the SC1 phase, which will provide insight into the distinction between each phase¹⁶.

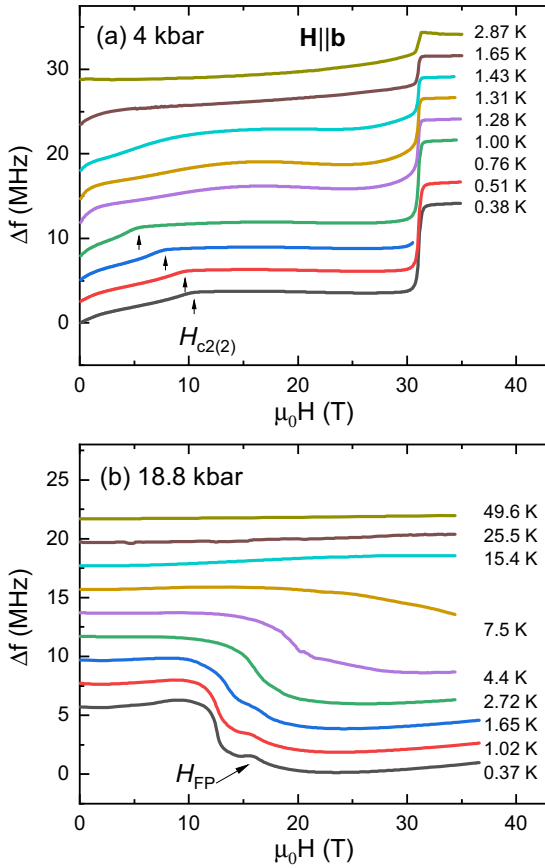


Fig. 2 Field evolution of magnetic susceptibility of UTe_2 under applied pressures. Tunnel diode oscillator (TDO) frequency variation of UTe_2 single crystal as a function of magnetic fields applied along the crystallographic b axis, under applied pressures of (a) 4 kbar and (b) 18.8 kbar. Transitions involving the SC2 superconducting phase are labeled as $H_{c2(2)}$ in panel (a), and crossovers to the field-polarized phases (see text) labeled as H_{FP} in panel (b). All curves are vertically shifted for presentation.

In contrast to the abrupt increase of Δf upon crossing H^* into the FP phase at lower pressures, the TDO signal exhibits a qualitatively different response in the high-pressure regime where superconductivity is completely suppressed. As shown in Fig. 2b, at 18.8 kbar Δf is almost field independent on increasing fields at 0.37 K until an abrupt drop occurs near 12 T. This drop reflects the decrease of skin depth, which can be confirmed by comparing with the decrease of resistance in our transport results. However, at slightly higher fields, we observe a small peak in Δf that does not match any observable feature in transport measurements. This peak suggests a metamagnetic transition at H_{FP} ($=15.5$ T at 0.37 K), indicating a crossover toward the FP phase.

Phase diagrams and GL theory

Compiling this data, we summarize the observed features and phase boundaries in both resistance and TDO measurements in Fig. 3. We identify five phases: two superconducting phases (labeled SC1 and SC2), the normal phase (labeled N), the FP phase, and the FM phase, which is only observed at 18.8 kbar. The first three phase diagrams (4, 8.5, and 14 kbar) show a smooth growth of the FP phase with pressure and the emergence of a more conventional (i.e., rounded) H - T boundary of the SC1 superconducting phase. In fact, the observable evolution of $H_{c2}(T)$ at 8.5 and 14 kbar indicates a putative $H_{c2}(0)$ critical point that would end within the FP phase were it not cut off by H^* .

We estimate these fields to be 72 T and 55 T for 8.5 kbar and 14 kbar, respectively (see Supplementary Fig. 5). In this pressure range, where the putative $H_{c2}(0)$ scale becomes comparable to the FP scale H^* , there are clear indications of an influence on the shape of the FP transition as noted above, despite its first-order nature (cf. hysteresis observed at base temperature shown in Fig. 3a, inset). Tracking the resistance peak H_p to fields above H^* traces a nonmonotonic curve that, when below T_c , mimics the extension of $H_{c2}(T)$ of the SC1 phase, again suggesting an intimate correlation between the two phases. This is corroborated by the fact that at 18.8 kbar, when superconductivity is completely suppressed, the onset of the FP phase shows a more conventional monotonic evolution with increasing field and temperature.

In an effort to explain the qualitative features of the phase diagram, we consider the phenomenological Ginzburg–Landau (GL) theory describing the superconducting order parameter η . For simplicity, we shall consider η to be single-component, relegating to the Supplementary Note the consideration of a multi-component order parameter proposed theoretically for UTe_2 ^{16,17} and corroborated by the recent specific heat measurements¹⁶. The free energy consists of three parts: $F = F_{sc}[\eta] + F_m[\mathbf{M}] + F_c[\eta, \mathbf{M}]$, with the first term describing the superconducting order parameter in the applied field¹⁸:

$$F_{sc}[\eta] = a(T)|\eta|^2 + \frac{\beta}{2}|\eta|^4 + K_{ij}(D_i\eta)^*(D_j\eta) + \frac{B^2}{8\pi}, \quad (1)$$

with $D_i = -i\nabla_i + \frac{2\pi}{\Phi_0}A_i$ denoting the covariant derivative in terms of the vector potential \mathbf{A} and $\Phi_0 = hc/2e$ the quantum of the magnetic flux, where $K_{ij} = \text{diag}\{K_x, K_y, K_z\}$ is the effective mass tensor in the orthorhombic crystal, $K_i^{-1} = 2m_i$. The simplest way, in which the superconducting order parameter couples to the field-induced microscopic magnetization \mathbf{M} , is via the biquadratic interaction $F_c = g\mathbf{M}^2|\eta|^2$, where the internal magnetic field $\mathbf{B}/\mu_0 = \mathbf{M} + \mathbf{H}$. The metamagnetic transition is described by the Landau theory of magnetization with a negative quartic term ($u, v > 0$):

$$F_m[\mathbf{M}] = \frac{\mathbf{M}^2}{2\chi(P, T)} + \frac{u}{4}\mathbf{M}^4 - \frac{v}{6}\mathbf{M}^6 - \mathbf{H} \cdot \mathbf{M}. \quad (2)$$

Taking the field $\mathbf{H}||\hat{b}$, and hence $\mathbf{A} = (Hz, 0, 0)$, we minimize the GL free energy to obtain the linearized gap equation of the form

$$-K_z \frac{d^2\eta}{dz^2} + K_x \left(\frac{2\pi H}{\Phi_0}\right)^2 z^2 \eta - a_0 \frac{(T_c - T)}{T_c} \eta + g\mathbf{M}^2 \eta = 0, \quad (3)$$

resulting in the eigenvalue spectrum similar to the problem of Landau levels for a particle in magnetic field¹⁹:

$$\hbar\omega_c \left(n + \frac{1}{2}\right) = a_0 \left(\frac{T_c - T}{T_c}\right) - g\mathbf{M}^2(T), \quad (4)$$

with the cyclotron frequency given by $\omega_c = 2eH\sqrt{K_x K_z}/c$. The upper critical field $H'_{c2}(T)$ is then determined from the lowest eigenvalue above:

$$H'_{c2}(T) = H_0 \left[\frac{T_c - T}{T_c} - \frac{g}{a_0} M^2(H_{c2}) \right], \quad (5)$$

where $H_0 = -T_c \frac{dH_{c2}}{dT} \Big|_{T_c}$ is related to the slope of H_{c2} at T_c in the absence of magnetization and $a_0 = \frac{\hbar^2}{2m\xi_0}$ is expressed in terms of the correlation length. The upshot of Eq. (5) is that the upper critical field is reduced from its bare value by the presence of the magnetization M . The latter is a function of the magnetic field, $M(H)$, to be determined from Eq. (2), and while its value depends on the phenomenological coefficients of the Landau theory, qualitatively, the metamagnetic transition results in a sudden increase of M at H^* (by $\Delta M \approx 0.6 \mu_B$ at $H^* = 34$ T at ambient pressure¹⁰). This then drives H'_{c2} down according to Eq. (5) and pins the upper critical field at the metamagnetic transition, explaining the sudden disappearance of superconductivity at the field H^* that marks the

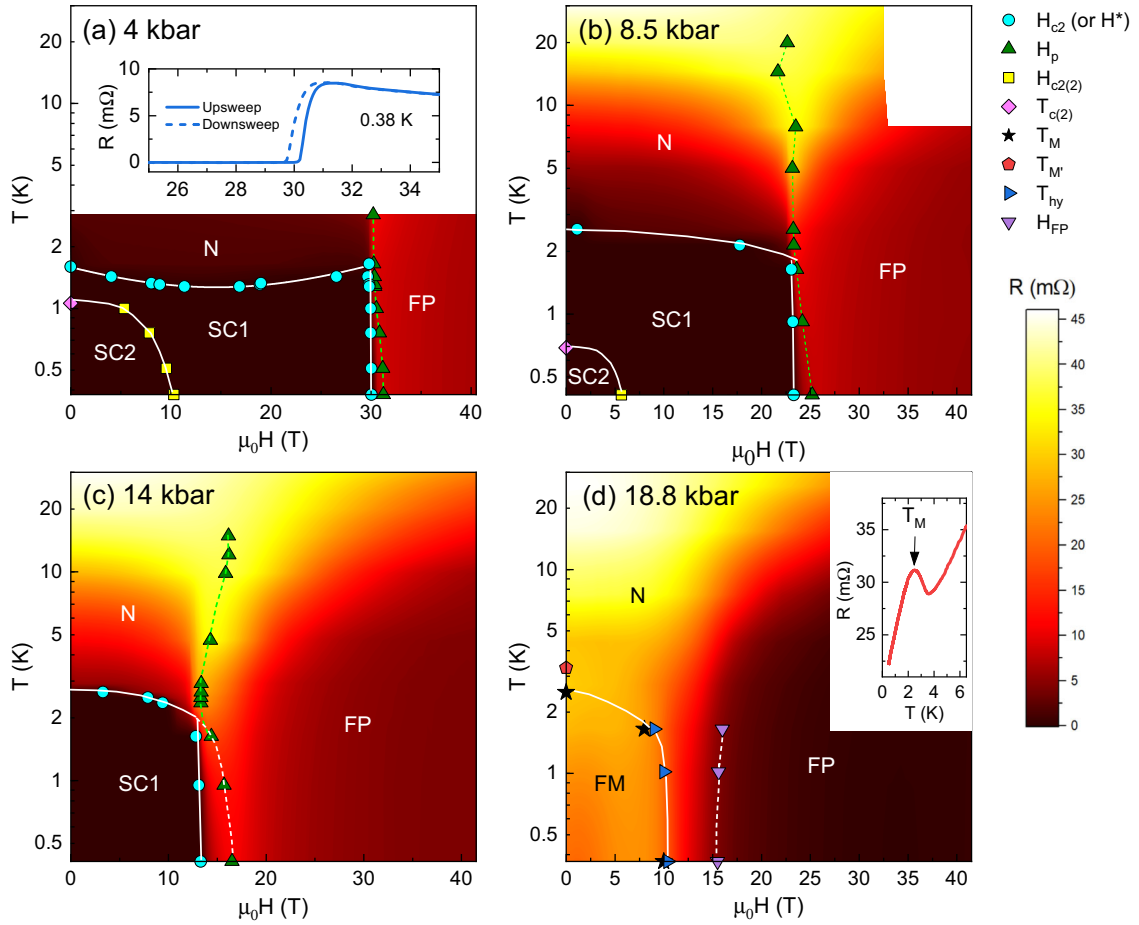


Fig. 3 Pressure evolution of magnetic field–temperature phase diagram of UTe_2 . Evolution of the magnetic field–temperature phase diagram of UTe_2 as a function of pressure for fields applied along the crystallographic b axis, with phase boundaries of superconducting (SC1 and SC2), normal (N), field-polarized (FP), and ferromagnetic (FM) phases determined by resistance and tunnel diode oscillator (TDO) data, and concomitant variations in resistance shown by background color contours. The inset of panel (a) shows the upswing and downswing of magnetoresistance around the metamagnetic transition. In panels (a–c), the cyan circles indicate the T_c transition into the SC1 superconducting phase obtained by field sweeps that are determined by zero-resistance criteria, and the green triangles label the position H_p of the peak in magnetoresistance. Yellow squares in panels (a, b) indicate critical field $H_{c2(2)}$ of the superconducting phase SC2 based on TDO measurements (cf. Fig. 2a), with pink diamonds indicating critical temperature $T_{c(2)}$ obtained from ref.¹³. In panel (d), the purple downward triangles label the crossover to the field-polarized state H_{FP} identified in TDO measurements (cf. Fig. 2b) while the blue rightward triangles label the demise of hysteresis H_{hy} in transport measurements. The black star identifies the transition T_M observed in the resistance temperature dependence (panel d, inset) while the red pentagon indicates the same transition measured in ref.¹³.

onset of the FP phase in Fig. 4c. Note that the above analysis focuses on the orbital effect of the applied magnetic field, since SC in UTe_2 is not Pauli-limited, presumably due to the equal-spin pairing nature of the pairing¹⁷.

It is worth discussing the value of H_{c2} , which is of the order $H_{c2} \sim 30$ T at low T and ambient pressure, much higher than would normally be inferred from $T_c \sim 2$ K. While the analysis of the linearized GL equation above only applies in the vicinity of T_c and cannot, strictly speaking, be used to infer the value of $H_{c2}(0)$ at zero temperature, the celebrated Werthamer–Helfand–Hohenberg theory²⁰ establishes a proportionality between the value of $H_{c2}(0)$ and the value H_0 in Eq. (5). We shall therefore use

$$H_0 = \frac{\Phi_0}{2\pi\hbar^2} \frac{a_0}{\sqrt{K_x K_z}} \equiv \frac{\Phi_0}{2\pi\hbar^2} a_0 m^*, \quad (6)$$

as a proxy for the upper critical field $H_{c2}(0)$ ($\Phi_0 = hc/2e$ is the flux quantum). We see that the role of the effective mass is played by $m^* = (K_x K_z)^{-1/2} \propto \sqrt{m_a m_c}$ and this helps explain the high observed value of H_{c2} in UTe_2 , as we show below. The key point is the quasi-two-dimensional nature of the Fermi surface sheets parallel to the c -axis, established by ARPES²¹ and ab initio

calculations^{17,22}, which can be approximated by writing the dispersion as

$$\epsilon_{\mathbf{k}} = \frac{\hbar^2}{2m_{ab}} \left[\left(k_a - \frac{\pi}{a} \right)^2 + \left(k_b - \frac{\pi}{b} \right)^2 \right] - 2T_c \cos(k_c d) - \mu, \quad (7)$$

where we have taken the in-plane mass to be isotropic for simplicity: $m_a = m_b = m_{ab}$, and T_c denotes the interlayer hopping strength along the c axis (d is the unit cell height). It follows that the carrier mass along k_c can be approximated by $m_c = \hbar^2/(2T_c d^2)$, which in turn means that the effective mass entering Eq. (6), $m^* \propto \sqrt{m_{ab}/(T_c d^2)}$. Smaller magnitude of the interlayer hopping T_c thus results in a higher value of H_0 in Eqs. (5) and (6). A more rigorous treatment based on the Green's function formalism reaches a qualitatively similar conclusion: $H_{c2}(0) \propto 1/T_c$ ²³, thus explaining the high values of H_{c2} in UTe_2 due to the quasi-two-dimensional nature of the Fermi surfaces. The key finding of the present study is that H_{c2} is in fact limited from above by the metamagnetic transition at field H^* , showcased by Eq. (5).

Focusing on the evolution of the ground state of UTe_2 with field and pressure (i.e., at our base temperature of ~ 0.4 K), we present

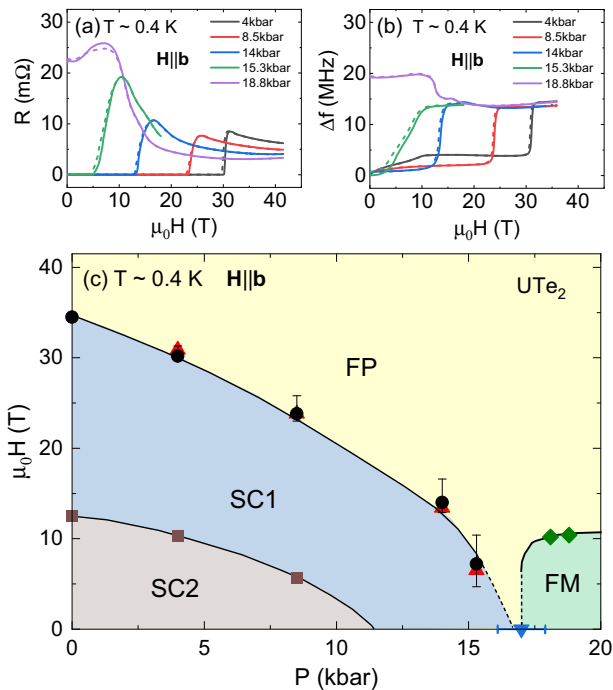


Fig. 4 Ground-state phase diagram of UTe_2 under applied field and pressure. Ground-state evolution of superconducting (SC1 and SC2), field-polarized (FP), and ferromagnetic (FM) phases in UTe_2 as a function of applied pressure and magnetic field applied along the crystallographic b axis. Panels (a) and (b) present resistance and tunnel diode oscillator (TDO) frequency variation, respectively, as functions of applied field at a fixed base temperature of the measurements. Both upsweeps (solid lines) and downsweeps (dashed lines) are plotted, indicating notable hysteresis. Note that in (b), all data are measured by a standard low-temperature-tuned TDO circuit, while the 15.3 kbar data were obtained using a room temperature-tuned circuit, and is therefore vertically scaled by a factor of 22 for comparison (see Supplementary Figs. 2 and 3c for more 15.3 kbar data). The resultant phase diagram at base temperature is presented in panel (c), where the phase boundary between SC1 and FP phases is determined by midpoints of resistance transitions (black circles, using an average of upsweep and downsweep curves) and TDO transitions (red triangles), with error bars indicating the width of transitions. Brown squares indicate the phase boundary of SC2 based on kinks in TDO frequency, and green diamonds indicate the magnetic transition determined from the resistance measurements. The blue upside-down triangle labels the critical pressure (P_c) where the superconductivity demises. Zero-pressure and zero-field data points are obtained from refs. ^{11,13}, respectively. All lines are guides to the eye.

summary plots of the resistance and TDO data as well as the ground-state field–pressure phase diagram in Fig. 4. As shown, the field boundaries of both SC1 and SC2 superconducting phases decrease monotonically with increasing pressure. However, we point out that, while the boundary of SC2 appears to be an uninterrupted upper critical field, that of SC1 is in fact the cut-off field H^* . It follows from Eq. (5) that this cut-off field is reduced compared to the putative H_{c2} , which would lie at higher fields if it were derived from an orbital-limited model without taking metamagnetic transition into account.

While the T_c of SC1 increases with pressure, the cutoff imposed by H^* introduces difficulty in determining whether its putative H_{c2} would also first increase with pressure. On the contrary, the unobstructed view of H_{c2} for SC2 shows a decrease with increasing pressure that is indeed consistent with the suggested decrease of the lower T_c transition observed in zero-field specific heat measurements¹³.

Between 15.3 and 18.8 kbar, the H^* cutoff is completely suppressed and the FM phase onsets. While it is difficult to obtain a continuous measure of the pressure evolution through that transition, the hysteresis in transport measurements is consistent with the low-field FM phase being the true magnetic ground state of the system, separate from the FP phase. The crossover toward the FP phase under field is entirely natural from the Landau theory perspective, since the external magnetic field is conjugate to the FM order parameter \mathbf{M} in Eq. (2), and the metamagnetic crossover at field H_M leads to a step-like increase in the magnetization, resulting in a small peak in TDO results.

This crossover boundary between the FM and FP phases appears much less sensitive to pressure for $P > P_c$, as evidenced by the minimal change in field value between 18.1 and 18.8 kbar. Because the experimental pressure cannot be tuned continuously, it is difficult to extract the behavior of the crossover boundary at P_c . However, the previously observed discontinuity between the FM and SC1 phases as a function of pressure¹² suggests that the FP phase should extend down to zero field at a critical point of $P_c \sim 17$ kbar, exactly where previous zero-field work has shown an abrupt cutoff of T_c and the onset of a non-superconducting phase¹³. This is different from the case of uranium-based ferromagnetic superconductors (UGe_2 , URhGe , UCoGe), where the superconductivity coexists with ferromagnetism. The distinctive behavior of UTe_2 is likely owing to a unique nature of its spin fluctuation spectrum, which may also benefit from reduced dimensions at high fields²³. In any case, as a nearly ferromagnetic superconductor, UTe_2 provides a unique platform for future investigation of the interplay between superconductivity and magnetic phases.

In summary, we have explored the pressure evolution of multiple superconducting and multiple magnetic phases of UTe_2 as a function of applied pressures and magnetic fields applied along the crystallographic b axis, where superconductivity is known to extend to the highest fields. The field-induced metamagnetic transition results in a field-polarized phase which cuts off superconductivity prematurely, as explained by a phenomenological Ginzburg–Landau theory. Under increasing pressure, the superconducting phase eventually becomes completely suppressed, at the critical pressure where we observe an onset of a distinct ferromagnetic-like ground state.

METHODS

Measurements

Single crystals of UTe_2 were synthesized by the chemical vapor transport method as described previously⁴. The crystal structure of UTe_2 is orthorhombic and centrosymmetric, and the magnetic easy axis is the a axis. Experimental measurements were conducted at the DC Field Facility of the National High Magnetic Field Laboratory (NHMFL) in Tallahassee, Florida, using a 41 T resistive magnet with a helium-3 cryostat. Resistance and magnetic susceptibility measurements were performed simultaneously on two individual samples from the same batch positioned in a non-magnetic piston-cylinder pressure cell. The pressure medium was Daphne 7575 oil, and the pressure was calibrated at low temperatures by measuring the fluorescence wavelength of ruby, which has a known temperature and pressure dependence^{24,25}. The TDO technique uses an LC oscillator circuit biased by a tunnel diode whose resonant frequency is determined by the values of LC components, with the inductance L given by a coil that contains the sample under study; the change of its magnetic properties results in a change in resonant frequency proportional to the magnetic susceptibility of the sample. Although not quantitative, the TDO measurement is indeed sensitive to the sample's magnetic response within the superconducting state where the sample resistance is zero^{26–28}. Both the current direction for the standard four-wire resistance measurements and the probing field generated by the TDO coil are along the crystallographic a axis (easy axis). The applied dc magnetic field was applied along the b axis (hard axis) for both samples (see Supplementary Fig. 1).

DATA AVAILABILITY

The data that support the findings of this study are available from the corresponding author upon reasonable request.

Received: 24 March 2020; Accepted: 9 September 2020;

Published online: 25 September 2020

REFERENCES

- Aoki, D., Ishida, K. & Flouquet, J. Review of U-based ferromagnetic superconductors: Comparison between UGe_2 , URhGe, and UCoGe. *J. Phys. Soc. Jpn.* **88**, 022001 (2019).
- Mineev, V. P. Reentrant superconductivity in URhGe. *Phys. Rev. B* **91**, 014506 (2015).
- Sundar, S. et al. Coexistence of ferromagnetic fluctuations and superconductivity in the actinide superconductor UTe_2 . *Phys. Rev. B* **100**, 140502 (2019).
- Ran, S. et al. Nearly ferromagnetic spin-triplet superconductivity. *Science* **365**, 684–687 (2019).
- Aoki, D. et al. Unconventional superconductivity in heavy fermion UTe_2 . *J. Phys. Soc. Jpn.* **88**, 043702 (2019).
- Metz, T. et al. Point-node gap structure of the spin-triplet superconductor UTe_2 . *Phys. Rev. B* **100**, 220504 (2019).
- Nakamine, G. et al. Superconducting properties of heavy fermion UTe_2 revealed by ^{125}Te -nuclear magnetic resonance. *J. Phys. Soc. Jpn.* **88**, 113703 (2019).
- Bae, S. et al. Anomalous normal fluid response in a chiral superconductor. Preprint at <https://arxiv.org/abs/1909.09032> (2019).
- Jiao, L. et al. Chiral superconductivity in heavy-fermion metal UTe_2 . *Nature* **579**, 523–527 (2020).
- Knebel, G. et al. Field-reentrant superconductivity close to a metamagnetic transition in the heavy-fermion superconductor UTe_2 . *J. Phys. Soc. Jpn.* **88**, 063707 (2019).
- Ran, S. et al. Extreme magnetic field-boosted superconductivity. *Nat. Phys.* **15**, 1250–1254 (2019).
- Ran, S. et al. Enhancement and reentrance of spin triplet superconductivity in UTe_2 under pressure. *Phys. Rev. B* **101**, 140503 (2020).
- Braithwaite, D. et al. Multiple superconducting phases in a nearly ferromagnetic system. *Commun. Phys.* **2**, 147 (2019).
- Knafo, W. et al. Magnetic-field-induced phenomena in the paramagnetic superconductor UTe_2 . *J. Phys. Soc. Jpn.* **88**, 063705 (2019).
- Miyake, A. et al. Metamagnetic transition in heavy fermion superconductor UTe_2 . *J. Phys. Soc. Jpn.* **88**, 063706 (2019).
- Hayes, I. M. et al. Weyl superconductivity in UTe_2 . Preprint at <https://arxiv.org/abs/2002.02539> (2020).
- Nevidomskyy, A. H. Stability of a nonunitary triplet pairing on the border of magnetism in UTe_2 . Preprint at <https://arxiv.org/abs/2001.02699> (2020).
- Mineev, V. P. & Samokhin, K. V. *Introduction to Unconventional Superconductivity* (CRC Press, 1999).
- Tinkham, M. *Introduction to Superconductivity* (Dover publications, 2004).
- Werthamer, N. R., Helfand, E. & Hohenberg, P. C. Temperature and purity dependence of the superconducting critical field, H_{c2} . III. Electron spin and spin-orbit effects. *Phys. Rev.* **147**, 295–302 (1966).
- Miao, L. et al. Low energy band structure and symmetries of UTe_2 from angle-resolved photoemission spectroscopy. *Phys. Rev. Lett.* **124**, 076401 (2020).
- Xu, Y., Sheng, Y. & Yang, Y.-F. Quasi-two-dimensional fermi surfaces and unitary spin-triplet pairing in the heavy fermion superconductor UTe_2 . *Phys. Rev. Lett.* **123**, 217002 (2019).
- Mineev, V. P. Reentrant Superconductivity in UTe_2 . *Jetp. Lett.* **111**, 715–719 (2020).
- Piermarini, G. J., Block, S., Barnett, J. D. & Forman, R. A. Calibration of the pressure dependence of the R 1 ruby fluorescence line to 195 kbar. *J. Appl. Phys.* **46**, 2774–2780 (1975).
- Ragan, D. D., Gustavsen, R. & Schiferl, D. Calibration of the ruby R 1 and R 2 fluorescence shifts as a function of temperature from 0 to 600 k. *J. Appl. Phys.* **72**, 5539–5544 (1992).
- Kim, H., Sung, N. H., Cho, B. K., Tanatar, M. A. & Prozorov, R. Magnetic penetration depth in single crystals of $SrPd_2Ge_2$ superconductor. *Phys. Rev. B* **87**, 094515 (2013).
- Cho, K. et al. Anisotropic upper critical field and possible Fulde-Ferrel-Larkin-Ovchinnikov state in the stoichiometric pnictide superconductor LiFeAs. *Phys. Rev. B* **83**, 060502 (2011).
- Prommapan, P. et al. Magnetic-field-dependent pinning potential in LiFeAs superconductor from its Campbell penetration depth. *Phys. Rev. B* **84**, 060509 (2011).

ACKNOWLEDGEMENTS

We thank H.-K. Wu and Y.-T. Hsu for useful discussions. This work was performed at the National High Magnetic Field Laboratory, which is supported by the National Science Foundation Cooperative Agreement No. DMR-1644779 and the State of Florida. Research at the University of Maryland was supported by AFOSR grant no. FA9550-14-1-0332, NSF grant no. DMR-1905891, the Gordon and Betty Moore Foundation's EPIQS Initiative through grant no. GBMF9071, NIST, and the Maryland Quantum Materials Center. D.J.C. acknowledges the support of the Anne G. Wylie Dissertation Fellowship. A.H.N. acknowledges the support from the Robert A. Welch Foundation grant C-1818 and the National Science Foundation grant no. DMR-1917511.

AUTHOR CONTRIBUTIONS

W.-C.L. and D.J.C. are co-first authors. W.-C.L., D.J.C., and J.P. conceived and designed the experiments. S.R. and N.P.B. synthesized the UTe_2 . I.-L.L. and S.R. helped characterize the samples. W.-C.L., D.J.C., and D.G. performed the measurements. A.H.N. provided the theoretical analysis. W.-C.L., D.J.C., H.K., A.H.N., N.P.B., and J.P. analyzed the data and wrote the paper.

COMPETING INTERESTS

The authors declare no competing interests.

ADDITIONAL INFORMATION

Supplementary information is available for this paper at <https://doi.org/10.1038/s41535-020-00270-w>.

Correspondence and requests for materials should be addressed to J.P.

Reprints and permission information is available at <http://www.nature.com/reprints>

Publisher's note Springer Nature remains neutral with regard to jurisdictional claims in published maps and institutional affiliations.



Open Access This article is licensed under a Creative Commons Attribution 4.0 International License, which permits use, sharing, adaptation, distribution and reproduction in any medium or format, as long as you give appropriate credit to the original author(s) and the source, provide a link to the Creative Commons license, and indicate if changes were made. The images or other third party material in this article are included in the article's Creative Commons license, unless indicated otherwise in a credit line to the material. If material is not included in the article's Creative Commons license and your intended use is not permitted by statutory regulation or exceeds the permitted use, you will need to obtain permission directly from the copyright holder. To view a copy of this license, visit <http://creativecommons.org/licenses/by/4.0/>.

© The Author(s) 2020

Tuning magnetic confinement of spin-triplet superconductivity: Supplementary Information

Wen-Chen Lin,¹ Daniel J. Campbell,¹ Sheng Ran,^{1,2,3} I-Lin Liu,^{1,2,3} Hyunsoo Kim,¹
Andriy H. Nevidomskyy,⁴ David Graf,⁵ Nicholas P. Butch,^{1,2} and Johnpierre Paglione*^{1,3,6}

¹*Maryland Quantum Materials Center, Department of Physics,
University of Maryland, College Park, MD 20742, USA*

²*NIST Center for Neutron Research, National Institute of Standards and Technology, Gaithersburg, MD 20899, USA*

³*Department of Materials Science and Engineering,
University of Maryland, College Park, MD 20742, USA*

⁴*Department of Physics and Astronomy, Rice University, Houston, Texas 77005, USA*

⁵*National High Magnetic Field Laboratory, Florida State University, Tallahassee, FL 32313, USA*

⁶*Canadian Institute for Advanced Research, Toronto, Ontario M5G 1Z8, Canada*

(Dated: September 6, 2020)

SUPPLEMENTARY NOTE

Details of the Ginzburg–Landau theory

In the main text, we have focused on a single-component superconducting order parameter for simplicity. At the same time, it has been suggested that the order parameter in UTe₂ may be two-component and have a non-zero magnetic moment of the Cooper pair aligned along the field direction – the so-called nonunitary triplet superconductor. This section analyzes the theoretical predictions for the upper critical field in this case.

Two-component order parameter

The odd-wave superconductor, such as believed to be the case in UTe₂, is described by an order parameter $\hat{\Delta}(\mathbf{k}) = i(\vec{d}_{\mathbf{k}} \cdot \vec{\sigma})\sigma_2$ expressed in terms of the \vec{d} -vector. The superconducting order parameter in a crystal can be decomposed into a linear superposition of the irreducible representations $\Gamma_i(\hat{\mathbf{k}})$ of the point-group symmetry:

$$\vec{d}(\mathbf{k}) = \sum_i \vec{\eta}_i \Gamma_i(\hat{\mathbf{k}}). \quad (1)$$

In the case of UTe₂, the point group D_{2h} contains only the one-dimensional representations, which would generically have different transition temperatures. As a result, the single-component order parameter, for which the Ginzburg–Landau (GL) theory has been presented in the main text, is expected to provide a sufficient description.

However, it has been pointed out that in a strong magnetic field, along for instance the crystallographic \hat{b} direction, the point group symmetry is lowered to C_{2h} , allowing for a linear superposition of the two irreducible representations, such as B_{1u} and B_{3u} [1]. Therefore, we shall consider a two-component order parameter which

encodes the expression for the \vec{d} -vector as a linear combination of these two irreducible representations [2]:

$$\vec{d}(\mathbf{k}) = \eta_x \hat{d}_{B_{3u}}(\mathbf{k}) + \eta_y \hat{d}_{B_{1u}}(\mathbf{k}) \quad (2)$$

Given the field in the \hat{b} direction, it is convenient to choose the coordinate system $(a, b, c) \rightarrow (y, z, x)$. In this notation, it was shown in Ref. 2 that the leading components of the B_{1u} and B_{3u} irreducible representations take the form:

$$\vec{d}_{B_{3u}}(\mathbf{k}) \sim \sin(k_b b) \hat{c} \propto (1, 0, 0) \quad (3)$$

$$\vec{d}_{B_{1u}}(\mathbf{k}) \sim \sin(k_b b) \hat{a} \propto (0, 1, 0), \quad (4)$$

so that the two-component order parameter transforms like the $\boldsymbol{\eta} = (\eta_x, \eta_y)$ vector in the xy -plane. Written explicitly as a matrix in the spin space, the superconducting order parameters takes on the following form:

$$\hat{\Delta} = i(\vec{d} \cdot \boldsymbol{\sigma})\sigma_2 = \Delta_0(\mathbf{k}) \begin{pmatrix} -\eta_x + i\eta_y & 0 \\ 0 & \eta_x + i\eta_y \end{pmatrix}. \quad (5)$$

Notice that the absence of the z -component of the d -vector (along the applied field direction) means that the order parameter matrix is diagonal, describing *equal-spin pairing* [2].

The most general Ginzburg–Landau theory allowed by orthorhombic symmetry can be split into two contributions: $F[\boldsymbol{\eta}] = F_0[\boldsymbol{\eta}] + F_B[\boldsymbol{\eta}]$, the first term being the zero-field Landau free energy

$$F_0[\boldsymbol{\eta}] = \alpha_x |\eta_x|^2 + \alpha_y |\eta_y|^2 + \frac{\beta_1}{2} (\boldsymbol{\eta} \cdot \boldsymbol{\eta}^*)^2 + \frac{\beta_2}{2} |\boldsymbol{\eta} \cdot \boldsymbol{\eta}|^2 \\ + \frac{\beta_x}{2} |\eta_x|^4 + \frac{\beta_y}{2} |\eta_y|^4, \quad (6)$$

where we have allowed for the xy anisotropy due to the orthorhombicity. In particular, $\alpha_x(T) \neq \alpha_y(T)$ allows, in principle, for different critical temperatures for the two components of $\boldsymbol{\eta}$, corroborated by two distinct signatures in the temperature dependence of the specific heat data [3].

The gradient terms [4] also contribute to the free energy, and become relevant when computing the upper critical field:

$$F_B[\boldsymbol{\eta}] = \frac{B^2}{8\pi} + K_1(D_i\eta_j)^*(D_i\eta_j) + K_2(D_i\eta_i)^*(D_j\eta_j) + K_3(D_i\eta_j)^*(D_j\eta_i) + F_{\text{ani}}[\boldsymbol{\eta}] \quad (7)$$

where the Einstein summation is implied over repeated indices $i, j = \{x, y\}$ and $D_i = -i\nabla_i + \frac{2\pi}{\Phi_0}A_i$ denotes the covariant derivative in the presence of the external vector potential \mathbf{A} . In addition to the above terms, the orthorhombic symmetry of the crystal allows to write down three more terms which we grouped into F_{ani} [4]:

$$F_{\text{ani}}[\boldsymbol{\eta}] = K_x(D_x\eta_1)^*(D_x\eta_1) + K_y(D_y\eta_2)^*(D_y\eta_2) + K_z(D_z\eta_i)^*(D_z\eta_i). \quad (8)$$

Note that the coefficients K_a play the role of $\hbar^2/2m_a$ in the traditional form often used to write down the GL equations, and the orthorhombic symmetry means that the effective mass tensor is anisotropic.

The applied magnetic field polarizes the electron spins in the normal state, resulting in the internal magnetization $\mathbf{M}(H)$. The free energy now contains additional

terms coupling the superconducting order parameter to the magnetization:

$$F_{\text{coupl}}[\boldsymbol{\eta}, \mathbf{M}] = g\mathbf{M}^2(\boldsymbol{\eta} \cdot \boldsymbol{\eta}^*) - w(\mathbf{M} + \mathbf{H}) \cdot (i\boldsymbol{\eta} \times \boldsymbol{\eta}^*), \quad (9)$$

The first term is the same as in the main text, whereas the second term describes the interaction of the total magnetic field $\mathbf{B} = \mu_0(\mathbf{M} + \mathbf{H})$ with the internal moment of the Cooper pair. This last term only appears in the *nonunitary* state where $\boldsymbol{\eta}^*$ is not collinear with $\boldsymbol{\eta}$, such as for instance

$$\boldsymbol{\eta}_{\text{chiral}} = (1, i\delta), \quad (10)$$

where δ is taken to be real (generically, $|\delta| \neq 1$ because of the absence of C_4 rotation in the xy -plane). Note that we do not need to consider the pair-breaking effect of the internal Zeeman field, due to the equal-spin pairing nature of the order parameter in Eq. (5). Indeed, this is consistent with the experimental evidence that H_{c2} exceeds the Pauli–Clogston limit in UTe₂ for field $H \parallel \hat{b}$.

We consider now the field along the \hat{z} (i.e. crystallographic \hat{b}) direction, as in the experiment, and choose the gauge where $\mathbf{A} = (-Hy, 0, 0)$. Differentiating with respect to η_j^* ($j = x, y$) and dropping the quartic terms in the free energy, we obtain the linearized GL equation in the form of two differential equations for η_x and η_y :

$$\begin{aligned} (K_{123} + K_x)D_x^2\eta_x + K_1D_y^2\eta_x + \tilde{\alpha}_x(T)\eta_x + (K_2D_xD_y + K_3D_yD_x)\eta_y - iw(M + H)\eta_y &= 0 \\ (K_{123} + K_y)D_y^2\eta_y + K_1D_x^2\eta_y + \tilde{\alpha}_y(T)\eta_y + (K_2D_xD_y + K_3D_yD_x)\eta_x + iw(M + H)\eta_x &= 0 \end{aligned} \quad (11)$$

where we have denoted $K_{123} \equiv K_1 + K_2 + K_3$ and

$$\tilde{\alpha}_i(T) = -\alpha_{0i} \left(\frac{T_c^{(i)} - T}{T_c^{(i)}} \right) + gM^2, \quad i = \{x, y\} \quad (12)$$

denotes the renormalized quadratic coefficients in the GL expansion due to the effect of coupling to the internal magnetization. Note that generically, the two transition temperatures T_c^x and T_c^y are not necessarily equal to each other, although the quartic coupling between the components of $\boldsymbol{\eta}$ means that in an experiment, both components become non-zero below the same physical T_c .

Unfortunately, the coupled differential equations (11) do not admit an analytical solution. Some progress can be made by searching for the solution in the form

$$\eta_i(x, y, z) \sim \tilde{\eta}(y)e^{ik_x x}e^{ik_z z}, \quad (13)$$

and ignoring the derivatives ∂_x in the Eqs. (11). Then,

the equations simplify:

$$\begin{aligned} -K_1\partial_y^2\eta_x(y) + (K_{123} + K_x) \left(\frac{2\pi H}{\Phi_0} \right)^2 y^2\eta_x(y) + \tilde{\alpha}_x(T)\eta_x - iw(M + H)\eta_y &= 0 \end{aligned} \quad (14)$$

$$\begin{aligned} -(K_{123} + K_y)\partial_y^2\eta_y(y) + K_1 \left(\frac{2\pi H}{\Phi_0} \right)^2 y^2\eta_y(y) + \tilde{\alpha}_y(T)\eta_y + iw(M + H)\eta_x &= 0 \end{aligned} \quad (15)$$

In order to allow for an analytical solution, let us limit the discussion to the case when $w = 0$ (i.e. the case of a unitary order parameter). Then, it is straightforward to find the solution for the upper critical field similar to the procedure in the main text:

$$\begin{aligned} H_{c2}^{(x)} &= \frac{\Phi_0}{2\pi\sqrt{K_1(K_{123} + K_x)}} \left[\alpha_{0x} \left(\frac{T_c^x - T}{T_c^x} \right) - gM^2(H) \right] \\ H_{c2}^{(y)} &= \frac{\Phi_0}{2\pi\sqrt{K_1(K_{123} + K_y)}} \left[\alpha_{0y} \left(\frac{T_c^y - T}{T_c^y} \right) - gM^2(H) \right]. \end{aligned} \quad (16)$$

Without carrying out the detailed calculation, which would depend on the phenomenological parameters of the GL theory and the details of the $M(H)$ dependence, it is clear that the H_{c2} is reduced for both components of the order parameter because of the presence of magnetization (g is positive in the free energy Eq. (9)). In particular, when $M(H)$ undergoes a metamagnetic transition at field H^* as in UTe_2 , the magnetization suddenly increases, and this has the potential of significantly reducing H_{c2} . We conclude that the behavior is qualitatively the same as described in the main text.

The physical H_{c2} is the larger of the two expressions in Eq. (16) above, and we further argue that $H_{c2}^x > H_{c2}^y$ in UTe_2 . Indeed, using the effective mass approximation to the electron dispersion Eq. (7) in the main text, we conclude that $K_x \sim t_c d^2 / \hbar^2$ is proportional to the inter-layer hopping strength t_c . That hopping is presumably very small due to the quasi-2D nature of the Fermi surfaces of UTe_2 , as remarked in the main text, and hence $K_x \ll K_y$, making $H_{c2}^x > H_{c2}^y$ in the limit of zero temperature, where we can neglect the difference between α_x and α_y . This is entirely consistent with the presence of two superconducting regions, denoted ‘‘SC1’’ and ‘‘SC2’’ in Figs. 3 and 4 in the main text, with SC1 having a higher H_{c2} . In our notation,

$$\text{SC1} : \boldsymbol{\eta}_1 \sim (1, 0) \propto B_{3u} \quad (17)$$

$$\text{SC2} : \boldsymbol{\eta}_2 \sim (1, \delta) \text{ or } (1, i\delta) \propto B_{3u} + B_{1u} \quad (18)$$

SUPPLEMENTARY FIGURES

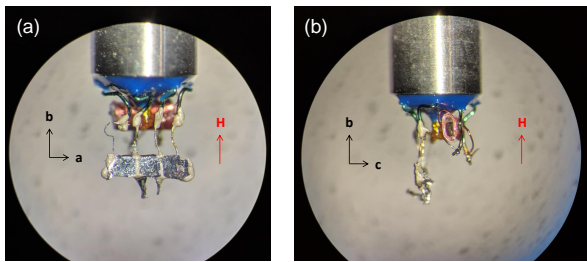


FIG. 1. (a) The front view (b) side view of UTe_2 samples mounted in the pressure cell. The lower sample was set up for four-probe resistance measurements and the upper sample was mounted inside a coil for TDO measurements. The crystallographic axis of the two samples are aligned in the same orientation as indicated by black arrows, with applied magnetic field directed vertically along the crystallographic b -axis.

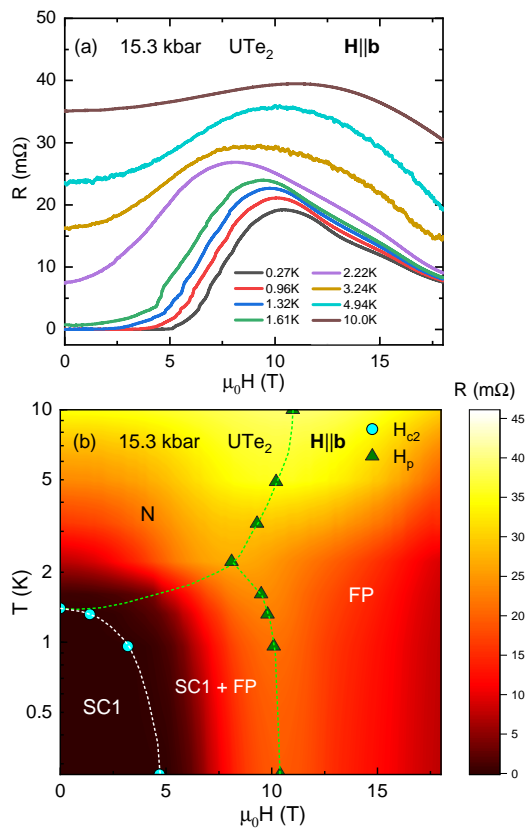


FIG. 2. (a) Magnetoresistance and (b) field-temperature phase diagram of a UTe_2 single crystal for fields applied along the crystallographic b -axis at 15.3 kbar. The cyan circles indicate the T_c transition into the SC1 superconducting phase obtained by field sweeps which are determined by zero-resistance criteria. Green triangles label the position H_p of the peak in magnetoresistance in panels (a). Under this pressure which is close to the critical pressure P_c , the transition between the SC1 phase and FP phase broadens, resulting in a wide regime of coexistence.

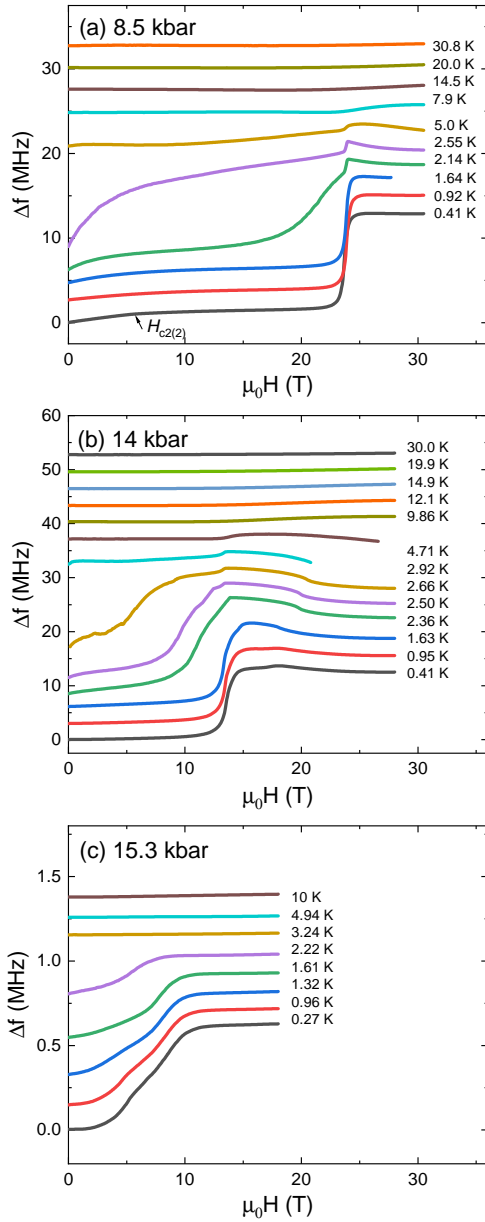


FIG. 3. Tunnel diode oscillator frequency variation of UTe_2 as a function of magnetic fields applied along the crystallographic b -axis, under applied pressures of (a) 8.5 kbar, (b) 14 kbar and (c) 15.3 kbar. All curves are vertically shifted for presentation.

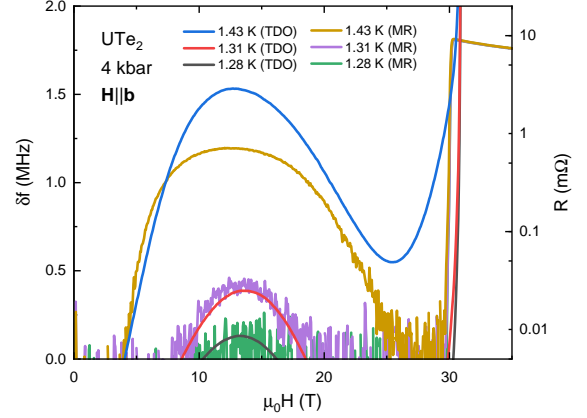


FIG. 4. Tunnel diode oscillator (TDO) frequency variation and magnetoresistance (MR) of a single crystal UTe_2 at 4 kbar with field parallel to the b -axis, where the latter is presented in log scale. As field increases, the MR data indicates reentrant superconductivity as the resistance changes from zero to nonzero and then back to zero. Simultaneously, the sign of TDO frequency variation shows consistent results going from negative (diamagnetism) to positive (paramagnetism), and then back to negative (diamagnetism). Near 30 T, the frequency variation changes sign again as the sample enters the field-polarized phase. Note that for the TDO data, an offset as well as a small linear background (0.1 MHz/T) have been applied to match the MR results.

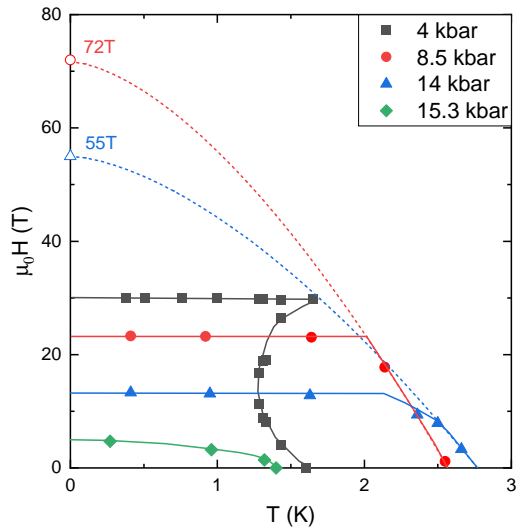


FIG. 5. The SC1 phase boundaries at different pressures with labelled putative upper critical fields. The uncommon shape of the phase boundary (i.e. flat top) suggests that the SC1 phase is truncated by the FP phase at the cutoff field H_c . The open labels indicate the putative upper critical fields which are calculated using the WHH equation, $H_{c2}(0) = -0.69 \times s \times T_c$. s represents the slope of phase boundary at T_c (i.e. $\frac{dH_{c2}}{dT}|_{T_c}$) which is estimated by considering the two closest data points to T_c . The resulting upper critical fields are 72 T and 55 T for 8.5 kbar and 14 kbar. The dashed-curved lines serve as guides to the eye.

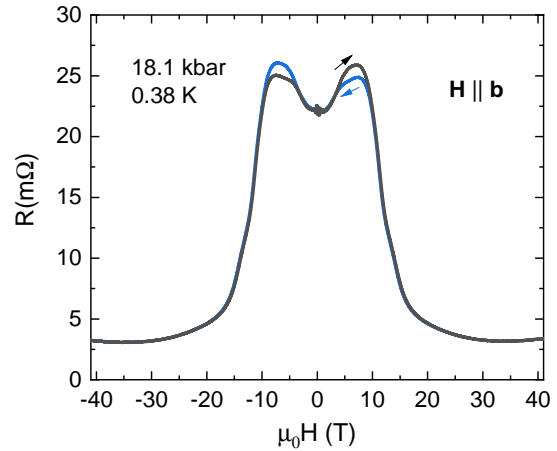


FIG. 6. The magnetoresistance of UTe_2 from 41 T to -41 T at 18.1 kbar. The hysteresis loops in both positive and negative field regions is consistent with the ferromagnetic-like ground state.

SUPPLEMENTARY REFERENCE

-
- [1] J. Ishizuka, S. Sumita, A. Daido, and Y. Yanase, *Phys. Rev. Lett.* **123**, 217001 (2019).
 - [2] A. H. Nevidomskyy, Preprint at <https://arxiv.org/abs/2001.02699> (2020).
 - [3] I. M. H. et al., Preprint at <https://arxiv.org/abs/2002.02539> (2020).
 - [4] V. P. Mineev and K. V. Samokhin, *CRC Press* (1999).